

Effects of QCD Resummation on W^+h and $t\bar{b}$ Production at the Tevatron

S. Mrenna*

*High Energy Physics Division
Argonne National Laboratory
Argonne, IL 60439*

C.-P. Yuan†

*Department of Physics and Astronomy
Michigan State University
East Lansing, MI 48824
(December 25, 2017)*

The resummation of multiple soft gluon emission affects the production rate and kinematic distributions of W^+h (where h is a Higgs boson) and $t\bar{b}$ pairs at the Tevatron with $\sqrt{s} = 2$ TeV. Using the Collins–Soper–Sterman resummation formalism, the production rate is enhanced over the next-to-leading-order (NLO) prediction by 2–3% for the W^+h process, for Higgs boson masses between 80–120 GeV, and over 3% for the $t\bar{b}$ process for $m_t = 175$ GeV. After resummation, the $t\bar{b}$ rate changes by 12–13% when m_t is varied by ± 5 GeV. Various kinematic distributions are presented for the individual final state particles and for the pair. The explicit radiation of hard gluons in NLO QCD is included also for the $t\bar{b}$ final state.

I. INTRODUCTION

The Tevatron collider at Fermilab, running at a center-of-mass energy $\sqrt{s} = 2.0$ TeV with a higher luminosity, will produce a sizeable number of electroweak gauge bosons at large invariant masses, which can subsequently decay to top quarks t or Higgs bosons h . Studying the properties of t and h are necessary to complete our understanding of the Standard Model (SM). The process $p\bar{p} \rightarrow W^{\pm*} \rightarrow W^{\pm}h$ is a promising avenue for detecting a light Higgs boson, which subsequently decays $h(\rightarrow b\bar{b})$ [1], or constraining the Higgs boson mass M_h . The process $p\bar{p} \rightarrow W^{+*} \rightarrow t\bar{b}$ ($W^{-*} \rightarrow \bar{t}b$) has been proposed to bound the CKM matrix element V_{tb} in a kinematic region where the parton distribution functions are well known [2]. After the decay $t \rightarrow bW^+(\bar{t} \rightarrow \bar{b}W^-)$, the second process is also a background to the first process, so it is interesting to study both in parallel. To determine the sensitivity of the Tevatron to M_h and V_{tb} or to observe any new physics effect in the $W^{\pm}b\bar{b}$ system, one has to know first the SM prediction for the production rate and the kinematic distributions of the final state system. The purpose of this study is to quantify the accuracy of the SM prediction for the next run at the Tevatron.

To test the SM or probe new physics, it is important to study the kinematics of the final state particles, like h and t . An accurate prediction of the rate and kinematics of particle production at hadron colliders must include initial and possibly final state radiation of gluons in QCD. Electroweak corrections are typically much smaller than higher order QCD corrections [3]. The effects of multiple soft gluon resummation on the kinematics of on shell W^{\pm} bosons and the leptonic decay products have been stud-

ied in some detail [4]. The situation is not so complete for off shell W^{\pm} boson production at large invariant mass. For the processes of interest, the initial and final (if any) state QCD corrections at NLO factorize separately. The predicted NLO rate for $W^{\pm}h$, with only initial state corrections, differs from the leading order (LO) rate by 36% for $M_h = 80$ GeV. The rate for $t\bar{b}$ production, with initial and final state corrections, differs by 60% for $m_t = 175$ GeV. Initial state soft gluon resummation may affect the size of these corrections and modify the kinematic distributions of the final state as expected from a NLO calculation. Furthermore, to accurately predict the kinematics of the $t\bar{b}$ final state at NLO, explicit hard gluon radiation must be included.

Sec. II contains a review of the Collins–Soper–Sterman (CSS) resummation formalism used in this study. We closely follow the notation used in Ref. [5]. In Sec. III, we present our numerical results for $q\bar{q}' \rightarrow W^{+*} \rightarrow W^+h$ production using this formalism. We show how to incorporate the effects of final state radiation in Sec. IV, and present numerical results for $q\bar{q}' \rightarrow W^{+*} \rightarrow t\bar{b}$. Finally, Sec. V contains our conclusions.

II. THE CSS RESUMMATION FORMALISM

Soft gluon resummation has been applied successfully to predict the rate and kinematics of electroweak gauge boson production at hadron colliders [5–8]. For W^{\pm} bosons, the CSS formalism has been applied only to leptonic final states. The same formalism can be directly applied to $W^{+*} \rightarrow W^+h$ production. However, for $W^{+*} \rightarrow t\bar{b}$ production, there are also singularities as-

sociated with the final state radiation which need to be handled separately.

The resummed differential cross section in the CSS formalism for the production of gauge boson V at a hadron collider with a center-of-mass energy \sqrt{s} is

$$\begin{aligned} & \left(\frac{d\sigma(h_1 h_2 \rightarrow V(\rightarrow d_1 d_2) X)}{dQ^2 dy dQ_T^2 d\phi_V d\cos\theta d\phi} \right)_{\text{resum}} = \\ & \frac{\beta}{96\pi^2 s} \frac{Q^2}{(Q^2 - M^2)^2 + M^2 \Gamma^2} \left\{ \int \frac{d^2 b}{(2\pi)^2} e^{i\vec{Q}_T \cdot \vec{b}} \right. \\ & \quad \times \sum_{j,k} \widetilde{W}_{jk}(b_*, Q, x_1, x_2, \theta, \phi, C_1, C_2, C_3) \\ & \quad \left. \times F_{jk}^{\text{NP}}(b, Q, x_1, x_2) + Y(Q_T, Q, x_1, x_2, \theta, \phi, C_4) \right\}, \quad (2.1) \end{aligned}$$

where Q, M, Γ, y, Q_T and ϕ_V are the mass, on shell mass, width, rapidity, transverse momentum, and azimuthal angle of V in the laboratory frame, θ and ϕ are the polar and azimuthal angle of the final state particle d_1 [see Eq. (2.8)] in the Collins-Soper frame [9], $x_1 = (Q/\sqrt{s}) \exp(y)$, $x_2 = (Q/\sqrt{s}) \exp(-y)$, and $\beta = 2p^*/Q$, where p^* is the momentum of d_1 and d_2 in the V rest frame. The renormalization group invariant \widetilde{W}_{jk} is given by

$$\begin{aligned} & \widetilde{W}_{jk}(b, Q, x_1, x_2, \theta, \phi, C_1, C_2, C_3) = \\ & \quad \exp\{-S(b, Q, C_1, C_2)\} |V_{jk}|^2 \\ & \quad \times \left\{ [(C_{jl} \otimes f_{l/h_1})(x_1) (C_{km} \otimes f_{m/h_2})(x_2) \right. \\ & \quad + (C_{kl} \otimes f_{l/h_1})(x_1) (C_{jm} \otimes f_{m/h_2})(x_2)] \\ & \quad \times g_L^2 f_S^2 \mathcal{H}_{jk}^S(Q, \cos\theta, m_{d_1}, m_{d_2}) \\ & \quad + [(C_{jl} \otimes f_{l/h_1})(x_1) (C_{km} \otimes f_{m/h_2})(x_2) \\ & \quad - (C_{kl} \otimes f_{l/h_1})(x_1) (C_{jm} \otimes f_{m/h_2})(x_2)] \\ & \quad \left. \times g_L^2 f_A^2 \mathcal{H}_{jk}^A(Q, \cos\theta, m_{d_1}, m_{d_2}) \right\}, \quad (2.2) \end{aligned}$$

where V_{jk} is a CKM matrix element for the initial state partons j and k , S is a Sudakov form factor, m_{d_1}, m_{d_2} are the final state masses, $\mathcal{H}^{S(A)}$ is a symmetric (antisymmetric) function in $\cos\theta$, $g_L^2 = G_F M_W^2 / \sqrt{2}$, $f_{S(A)}$ is a coupling for the symmetric (antisymmetric) function, and \otimes denotes the convolution integral of the Wilson coefficients C and the parton distribution functions (PDF's)

$$\begin{aligned} & (C_{jl} \otimes f_{l/h_1})(x_1) = \\ & \int_{x_1}^1 \frac{d\xi_1}{\xi_1} C_{jl}(\frac{x_1}{\xi_1}, b, \mu = \frac{C_3}{b}, C_1, C_2) \\ & \quad \times f_{l/h_1}(\xi_1, \mu = \frac{C_3}{b}). \quad (2.3) \end{aligned}$$

For the processes under consideration, $j = q, k = \bar{q}'$, excluding t quarks. The dummy indices l and m sum

over quarks and anti-quarks or gluons, and summation on double indices is implied. The angular function $\mathcal{H}^{S(A)}$ and coupling constants $f_{S(A)}$ in Eq. (2.2) for the $d_1 = W^+$, $d_2 = h$ final state are

$$\begin{aligned} & (M_W^2/Q^2) \left[2 + (p^*/M_W)^2 (1 - \cos^2\theta) \right], (S) \\ & \quad 0, (A) \\ & f_S^2 = \sqrt{2} G_F M_W^2, f_A^2 = 0, \end{aligned}$$

and for the $d_1 = t$, $d_2 = \bar{b}$ final state are

$$\begin{aligned} & 3 \left[(1 - (m_t^2 - m_b^2)^2/Q^4 + (2p^*/Q)^2 \cos^2\theta) \right], (S) \\ & \quad 3 [(4p^*/Q) \cos\theta], (A) \\ & f_S^2 = f_A^2 = g_L^2 |V_{tb}|^2. \end{aligned}$$

The Sudakov form factor $S(b, Q, C_1, C_2)$ in Eq. (2.1) is defined as

$$S(b, Q, C_1, C_2) = \int_{C_1^2/b^2}^{C_2^2 Q^2} \frac{d\bar{\mu}^2}{\bar{\mu}^2} \left[\ln \left(\frac{C_2^2 Q^2}{\bar{\mu}^2} \right) A(\alpha_s(\bar{\mu})) + B(\alpha_s(\bar{\mu})) \right], \quad (2.4)$$

where α_s is the strong coupling constant, and the functions A, B and the Wilson coefficients C_{jl} were given in Ref. [5]. The constants C_1, C_2 and $C_3 \equiv \mu b$ arise when solving the renormalization group equation for the \widetilde{W}_{jk} . The canonical choice of these renormalization constants is $C_1 = C_3 = 2 \exp(-\gamma_E) \equiv b_0$ and $C_2 = 1$, where γ_E is the Euler constant. In general, the choice $C_1 = C_2 b_0$ and $C_3 = b_0$ eliminates large constant factors in the expressions for the A, B and C_{jk} functions. As shown in Eq. (2.4), the upper limit of the integral for calculating the Sudakov factor is $\bar{\mu} = C_2 Q$, which sets the scale of the hard scattering process when evaluating the renormalization group invariant quantity \widetilde{W}_{jk} , as defined in Eq. (2.2). The lower limit $\bar{\mu} \equiv C_1/b = b_0/b$ determines the onset of nonperturbative physics. When integrated over the impact parameter b , the \widetilde{W} term is referred to as the CSS piece.

The Y piece in Eq. (2.1) is defined as

$$\begin{aligned} & Y(Q_T, Q, x_1, x_2, \theta, \phi, C_4) = \\ & \int_{x_1}^1 \frac{d\xi_1}{\xi_1} \int_{x_2}^1 \frac{d\xi_2}{\xi_2} \sum_{N=1}^{\infty} \left[\frac{\alpha_s(C_4 Q)}{\pi} \right]^N \\ & \quad \times f_{l/h_1}(\xi_1; C_4 Q) R_{lm}^{(N)}(Q_T, Q, \frac{x_1}{\xi_1}, \frac{x_2}{\xi_2}, \theta, \phi) \\ & \quad \times f_{m/h_2}(\xi_2; C_4 Q), \quad (2.5) \end{aligned}$$

where the functions $R_{lm}^{(N)}$ only contain contributions less singular than $Q_T^{-2} \times (1 \text{ or } \ln(Q^2/Q_T^2))$ as $Q_T \rightarrow 0$ in the fixed order perturbative calculation. The perturbative expansion is optimized by choosing $C_4 = 1$, so that the scale of the Y piece is Q .

In Eq. (2.1), the impact parameter b is to be integrated from 0 to ∞ . However, for $b \geq b_{\text{max}}$, which corresponds

to an energy scale much less than $1/b_{\max}$, the QCD coupling α_s becomes so large that a perturbative calculation is no longer reliable. The nonperturbative physics in this region is described by an empirically fit function F^{NP} with the general structure

$$F_{jk}^{\text{NP}}(b, Q, Q_0, x_1, x_2) = \exp \left\{ -\ln \left(\frac{Q^2}{Q_0^2} \right) h_1(b) - h_{j/h_1}(x_1, b) - h_{k/h_2}(x_2, b) \right\}. \quad (2.6)$$

The functions h_1 , h_{j/h_1} and h_{k/h_2} cannot be calculated using perturbation theory and must be measured experimentally. Furthermore, \widetilde{W} is evaluated at b_* , instead of b , with

$$b_* = \frac{b}{\sqrt{1 + (b/b_{\max})^2}} \quad (2.7)$$

such that b_* never exceeds b_{\max} .

To obtain the kinematics of the final state products d_1 and d_2 from $V^* \rightarrow d_1 d_2$, we transform the four momentum of d_1 ($\equiv p^\mu$) and d_2 ($\equiv \bar{p}^\mu$) from the Collins–Soper frame to the laboratory frame. The resulting expressions are

$$\begin{aligned} p^\mu &= \frac{Q}{2} \left(\frac{q^\mu}{Q} + \sin \theta \cos \phi X^\mu + \sin \theta \sin \phi Y^\mu + \cos \theta Z^\mu \right), \\ \bar{p}^\mu &= q^\mu - p^\mu, \\ q^\mu &= (M_T \cosh y, Q_T \cos \phi_V, Q_T \sin \phi_V, M_T \sinh y), \\ X^\mu &= -\frac{Q}{Q_T M_T} (Q_+ n^\mu + Q_- \bar{n}^\mu - \frac{M_T^2}{Q^2} q^\mu), \\ Y^\mu &= \epsilon^{\mu\nu\alpha\beta} \frac{q_\nu}{Q} Z_\alpha X_\beta, \\ Z^\mu &= \frac{1}{M_T} (Q_+ n^\mu - Q_- \bar{n}^\mu), \end{aligned} \quad (2.8)$$

with $q^\mu = (q^0, q^1, q^2, q^3)$, $Q_\pm = (q^0 \pm q^3)/\sqrt{2}$, $Q = \sqrt{q^2}$, $M_T = \sqrt{Q^2 + Q_T^2}$, $y = \ln(Q_+/Q_-)/2$, $n^\nu = (1, 0, 0, 1)/\sqrt{2}$, $\bar{n}^\nu = (1, 0, 0, -1)/\sqrt{2}$, and $\epsilon^{0123} = -1$. In the Collins–Soper frame of reference, the W^* is at rest and the z axis is defined as the bisector of the angle formed by \vec{p}_{h_1} and $-\vec{p}_{h_2}$, where \vec{p}_{h_1} and \vec{p}_{h_2} are the momentum of the initial state hadrons. As suggested by the notation, X^μ, Y^μ, Z^μ are the transformations of the $x-, y-, z-$ components of d_1 , respectively, from the CSS to the laboratory frame. Similar expressions can be derived when there are more particles in the final state as discussed in Sec. IV.

III. THE NUMERICAL RESULTS OF INITIAL STATE RESUMMATION

In this section, we present numerical results for the $q\bar{q}' \rightarrow W^{+*} \rightarrow W^+ h$ process after applying the resummation formalism outlined in the previous section at the upgraded Tevatron with $\sqrt{S} = 2.0$ TeV. For these results, we have assumed $m_t = 175$ GeV and $m_b = 5$ GeV and several values of the Higgs boson mass M_h . In the following, distributions will be shown for $W^+ h$ production only. This allows us to exhibit asymmetries along the beam axis. The distributions for $W^- h$ production can be obtained by reflection about rapidity $y = 0$.

As explained in the previous section, the CSS piece depends on the renormalization constants $C_1, C_2 = C_1/b_0$ and $C_3 = b_0$, as well as a few other implicit parameters. The choice of C_2 indicates that the hard scale of the process is $C_2 Q$. For this study, we use $C_2 = 1$, which fixes the scale at the off shell gauge boson mass. We also use the CTEQ3M NLO PDF's [10], the NLO expression for α_s , and the non-perturbative function [11]

$$F^{\text{NP}}(b, Q, Q_0, x_1, x_2) = \exp \left\{ -g_1 b^2 - g_2 b^2 \ln \left(\frac{Q}{2Q_0} \right) - g_3 g_3 b \ln(100x_1 x_2) \right\}, \quad (3.1)$$

where $g_1 = 0.11 \text{ GeV}^2$, $g_2 = 0.58 \text{ GeV}^2$, $g_3 = -1.5 \text{ GeV}^{-1}$ and $Q_0 = 1.6 \text{ GeV}$. The choice $b_{\max} = 0.5 \text{ GeV}^{-1}$ was used in this fit. * Finally, the CSS piece is fixed by specifying the order in α_s of the A, B and C_{jk} functions. We adopt the notation (M, N) to represent the order in α_s of $A^{(M)}, B^{(M)}$ and $C_{jk}^{(N)}$. The choice $(1, 0)$, for example, means that A and B are calculated to order α_s , while $C_{jk}(z)$ is either 0 or $\delta(1-z)$ depending on j and k .

The CSS piece alone gives an accurate description of the kinematics of the off shell W^+ boson for $Q_T \ll Q$. However, because of the soft gluon approximations made in the resummation, the CSS piece becomes negative when $Q_T \sim Q$. The regular Y piece accounts for terms neglected in \widetilde{W} at any fixed order in perturbation theory. The sum $\text{CSS} + Y$ can become negative for $Q_T \sim Q$, but, when integrated over Q_T from 0 to Q , returns the NLO result for the total cross section and Q distribution. We have checked this agreement numerically. Since the Q_T distribution is a physical observable, negative differential cross sections are not allowed. Therefore, when $\text{CSS} + Y$ no longer gives an accurate description of the physics, one should use a prediction at a fixed order in α_s , since the perturbation series in α_s gives a better convergence for $Q_T \sim Q$. Switching between the two formalisms requires a matching prescription. Our prescription is to

* These values were fit for CTEQ2M PDF and $C_2=1$, and in principle should be refit for CTEQ3M PDF.

switch smoothly to the fixed order differential cross section once $\text{CSS}+Y$ becomes smaller than the fixed order prediction as $Q_T \simeq Q$. The cross section after matching, then, gives a different prediction than the NLO result. We refer to a full resummed calculation, including the Y piece and matching, as $\text{CSS}(M,N)$, where (M,N) specify the order of the A, B , and C functions.

Part of the next-to-next-to-leader-order (NNLO) prediction for W^* production can be included through $A^{(2)}$ and $B^{(2)}$ in Eq. (2.4) [5]. When matching to the $\text{CSS}(1,1)$ ($\text{CSS}(2,1)$) calculation, we use the NLO (NNLO) perturbative prediction for high transverse momentum W^\pm boson production [12]. We apply the results of our calculations to study the total rate and the kinematic distributions of the W^+h pair and the individual W^+ or h produced in hadron collisions. These do not include any final state effects.

The effects of resummation on the total production rate are illustrated in Table I, which compares LO, NLO, the CSS formalism with A, B , and C functions of order (1,1) and matching, and the CSS formalism of order (2,1) and matching. The LO result uses the CTEQ3L PDF's. The $\text{CSS}(1,1)$ and $\text{CSS}(2,1)$ predictions are indistinguishable once matching is used, and reveal a slight enhancement over the NLO prediction. We interpret the difference between the NLO and CSS predictions as a gauge of the intrinsic theoretical uncertainty in the total rate up to order α_s^2 . Referring to Table I, higher order corrections to the NLO prediction could be as large as 2–3%. There will also be some uncertainty from varying the PDF, but we have not investigated this.

The effect of resummation on various kinematic distributions are displayed in Figs. 1–5. Distributions for the individual W^+ and h are basically changed in rate, but not in shape, compared to the LO and NLO predictions (see Figs. 2–4). On the scale of the figures, there is not a significant difference between $\text{CSS}(2,1)$ and $\text{CSS}(1,1)$, so we do not include $\text{CSS}(1,1)$ in these figures. However, those observables which depend on the kinematics of the pair are sensitive to the order of resummation. For the purposes of generating NLO distributions, a Q_T cut of .8 GeV is imposed to separate the real emission from the virtual corrections. Q_T is the transverse momentum of the virtual W^{+*} boson, or, equivalently, the W^+h pair, since we do not include any final state corrections. Near this cut, we have little confidence in the ability of the NLO calculation to accurately describe the Q_T distribution. Even far from this cut, however, the NLO Q_T distribution grossly underestimates the Q_T distribution as expected from resummation (see Fig. 1). At high Q_T , $\text{CSS}(2,1)$ predicts an enhancement over $\text{CSS}(1,1)$, which means more hard gluon radiation. Also, $\text{CSS}(2,1)$ predicts a large azimuthal angle separation ($\Delta\phi^{W^+h}$) between W^+ and h (see Fig. 5).

IV. INITIAL STATE RESUMMATION WITH EXPLICIT FINAL STATE RADIATION

Using the same approach discussed in Section III, we have also studied the effects of soft gluon resummation on the process $q\bar{q}' \rightarrow W^{+*} \rightarrow t\bar{b}$ for several values of $m_t = 170, 175, 180$ GeV. The presence of hadronic final states, however, adds a complication. In Ref. [13], the CSS formalism was applied to the production of $t\bar{t}$ pairs at the Tevatron. The effects of final state radiation were incorporated in this result by resumming all of the final state logarithms that behave like $Q_T^{-2} \ln(Q_T/Q)^2$ and adding these coherently to those similar terms from the initial state. This was justified on the grounds that color links the initial state to the final state at NLO. Also, previous studies of top quark decay at NLO show that most gluon radiation occurs off the b quark line, so that final state radiation off the t quark line is a smaller effect [14]. For the production of a hadronic final state through an s channel W^* boson, there is no interference at NLO between Feynman diagrams with initial and final state QCD corrections, so that the effect of initial state corrections can be calculated separately from final state corrections. To calculate the total cross section for $W^* \rightarrow t\bar{b}$, we resum the initial state multiple soft gluon radiation and include the effect of QCD radiation at NLO for hadronic final states by multiplying the production rate for $p\bar{p} \rightarrow W^{+*} \rightarrow t\bar{b}$ by a factor of $K_{\text{fsr}}(Q^2)$, a function of only Q^2 once the masses of t and \bar{b} are fixed [15].

The effects of initial state resummation with the final state QCD correction K_{fsr} on the total production rate are summarized in Table II, which compares the LO, NLO, $\text{CSS}(1,1)$, and $\text{CSS}(2,1)$ predictions for various values of m_t . For $m_t = 175$ GeV, the enhancement from the CSS formalism over NLO is about 3.5%, which is an estimate of the effects of higher order corrections. The enhancement over the LO result is 66%. As a comparison, the variation in rate from a change in m_t by ± 5 GeV around a nominal value of 175 GeV is 12–13%. Our NLO correction from initial state radiation, which is 37% for $m_t = 175$ GeV, agrees with Ref. [3]. However, our NLO correction from final state radiation, which is an additional 17% enhancement, is about 3.4% higher than Ref. [3]. The enhancement of the resummed result over the NLO result is based on *our* calculation of the NLO rate. A study of the kinematic distributions of the final state particles t and \bar{b} at NLO in QCD requires a separation of the states with and without explicit hard gluon radiation. While K_{fsr} can predict the change in rate from final state radiation, it has integrated out the kinematics of the final state particles. To remedy this situation, so that we can study the explicit final states $t\bar{b}$ and $t\bar{b}g$, we calculate the correction function $K_{\text{fsr}}^{(3)}(Q^2, E_g^{\text{min}})$ for the exclusive process $W^{+*} \rightarrow t\bar{b}g$ using a minimum gluon energy E_g^{min} as a regulator. The effect of the regulator on the exclusive process $W^{+*} \rightarrow t\bar{b}$ can be calculated using $K_{\text{fsr}}^{(2)}(Q^2, E_g^{\text{min}}) = K_{\text{fsr}}(Q^2) - K_{\text{fsr}}^{(3)}(Q^2, E_g^{\text{min}})$. This

is a practical method as long as the value of E_g^{\min} transformed to the laboratory frame does not exceed the lowest jet energy used by an experiment in an analysis. In our numerical results, $E_g^{\min} = 1$ GeV. [†]

Figs. 6–11 show the effects of initial state resummation and final state NLO QCD radiation on the kinematic distributions of the t , \bar{b} , and the pair $t\bar{b}$. The Q_T distribution in Fig. 6 is still the transverse momentum of the virtual W^{+*} boson, so it does not depend on the separation of final states with and without hard gluon radiation. For this study, the t and \bar{b} are produced on shell and treated at the parton level. No jet definition is used to combine the hard gluon with t or \bar{b} partons. We present results for the resummation calculations CSS(2,1). On the scale of these figures, there is no significant difference between CSS(2,1) and CSS(1,1). For comparison, we show the distribution expected using two body kinematics for $t\bar{b}$ but still using the full final state correction K_{fsr} . The difference between this distribution, denoted as 2–body in the figures, and the resummed curve indicates the size of the “hard” gluon effects, that is, the contribution from $t\bar{b}g$ for a fixed E_g^{\min} . When we feel a comparison is useful, we also include the LO prediction. For the kinematics of the individual t or \bar{b} , the effect on the shape of distributions from final state radiation is important, more so than from the resummation (see Figs. 7–11), and we do not see a noticeable difference between the NLO and resummed curves with our choice of E_g^{\min} . The kinematics of the $t\bar{b}$ pair, however, are sensitive to the initial state gluon radiation (see Figs. 6 and 12). This can be understood as follows. Similar to the W^+h final state, initial state gluon radiation only affected distributions of the $t\bar{b}$ pair. Why is this so? This is mainly determined by the kinematics and the nature of the radiation divergence for the initial and final states. In the initial state, the partons are collinear with the beam axis, and the leading divergence is both soft and collinear. As a result, the Q_T distribution (see Fig. 6) peaks around a few GeV, while the rapidity of the pair is very central. The LO distribution for P_T^t , in contrast, peaks near 30 GeV. Therefore, there is little effect of the Q_T smearing on P_T^t . The same argument can be applied to the t rapidity distribution y^t . The final state radiation, on the other hand, only produces soft divergences, and the final state particles tend to be central and not collinear with the beam. Therefore, distributions with respect to the beam axis, such as P_T^t and P_T^b , are more sensitive to the final state effects.

[†] As discussed in Ref. [4], if the kinematic cuts imposed to select the signal events are correlated with the transverse momentum Q_T of the virtual W boson, then the distributions predicted by the NLO and the resummed calculations will be different. The difference is the largest near the boundary of the phase space, such as in the large rapidity region.

V. CONCLUSIONS

We have studied the effects of QCD resummation in the CSS formalism on the production of W^{+*} bosons at the Tevatron and the kinematics of the final state products W^+h and $t\bar{b}$. Understanding the W^+h production rate is important for quantifying the Higgs boson discovery potential of the Tevatron. We find an increase in rate over the LO result of 40% for $M_h = 80$ GeV, and 29% for $M_h = 120$ GeV. This is only slightly higher than the NLO prediction, even though we have included part of the NNLO correction. Therefore, we estimate the effect of higher order QCD corrections to be 2–3% over the NLO prediction. The shape of kinematic distributions of the W^+ and h are not significantly altered from the LO or NLO predictions. The kinematics of the W^+h pair, however, can only be accurately predicted using a resummed calculation, and might be useful to distinguish signal from background.

Understanding the $t\bar{b}$ production rate is important for the determination of the CKM matrix element V_{tb} . We have included the explicit radiation of final state gluons at NLO, so that we predict the kinematics of $t\bar{b}$ and $t\bar{b}g$ events. We find an increase in rate over the LO result of 66% for $m_t = 175$ GeV, and we estimate the effect of higher order corrections to be more than 3% over the NLO result. The total production rate changes 12–13% when m_t is varied by ± 5 GeV. The effects of final state radiation are more important than initial state resummation for the kinematics of the individual t or \bar{b} . With explicit gluon radiation, the P_T spectrum of both t and \bar{b} are harder, so that the b tagging efficiency should be higher. The kinematics of the $t\bar{b}$ pair are also interesting observables.

ACKNOWLEDGMENTS

We thank C. Balazs for discussions. This work was supported in part by NSF grant PHY-9507683 and by DOE grant W-31-109-ENG-38.

* Electronic mail: mrenna@hep.anl.gov

† Electronic mail: yuan@pa.msu.edu

- [1] A. Stange, W. Marciano, and S. Willenbrock, Phys. Rev. **D49**, 1354 (1994); **D50**, 4491 (1994).
- [2] T. Stelzer and S. Willenbrock, Phys. Letts. **B357**, 125 (1995).
- [3] M.C. Smith and S. Willenbrock, Phys. Rev. **D54**, 6696 (1996).
- [4] C. Balazs, J. Qiu, and C.-P. Yuan, Phys. Letts. **B355**, 548 (1995).

- [5] J. Collins, D. Soper and G. Sterman, Nucl. Phys. **B250**, 199 (1985).
 [6] G. Altarelli, R.K. Ellis, M. Greco, G. Martinelli, Nucl. Phys. **B246**, 12 (1984).
 [7] J. Collins and D. Soper, Nucl. Phys. **B193**, 381 (1981); Erratum **B213**, 545 (1983); **B197**, 446 (1982).
 [8] P.B. Arnold and R.P. Kauffman, Nucl. Phys. **B349**, 381 (1991).
 [9] J. Collins and D. Soper, Phys. Rev. **D16**, 2219 (1977).
 [10] H.L. Lai, J. Botts, J. Huston, J.G. Morfin, J.F. Owens, J.W. Qiu, W.K. Tung, H. Weerts, MSU preprint MSU-HEP-41024, 1994 (unpublished).
 [11] G.A. Ladinsky and C.-P. Yuan, Phys. Rev. **D50**, 4239 (1994).
 [12] P. Arnold and M. Reno, Nucl. Phys. **B319**, 37 (1989); Erratum **B330**, 284 (1990).
 [13] S. Mrenna and C.-P. Yuan, Phys. Rev. **D55**, 120 (1997).
 [14] S. Mrenna and C.-P. Yuan, Phys. Rev. **D46**, 1007 (1992).
 [15] T.H. Chang, K.J.F. Gaemers, and W.L. van Neerven, Nucl. Phys. **B202**, 407 (1982).

Order	Higgs Mass (GeV)		
	80	100	120
CSS (2,1)	.305	.154	.083
CSS (1,1)	.304	.154	.083
NLO	.296	.149	.081
LO	.218	.109	.059

TABLE I. Total cross section in pb for W^+h production at the Tevatron in various approximations for $M_h=80,100$, and 120 GeV.

Order	Top Mass (GeV)		
	170	175	180
CSS (2,1)	.541	.478	.423
CSS (1,1)	.541	.477	.423
NLO	.523	.462	.409
LO	.327	.288	.255

TABLE II. Total cross section in pb for $t\bar{b}$ production at the Tevatron in various approximations for $m_t=170,175$, and 180 GeV.

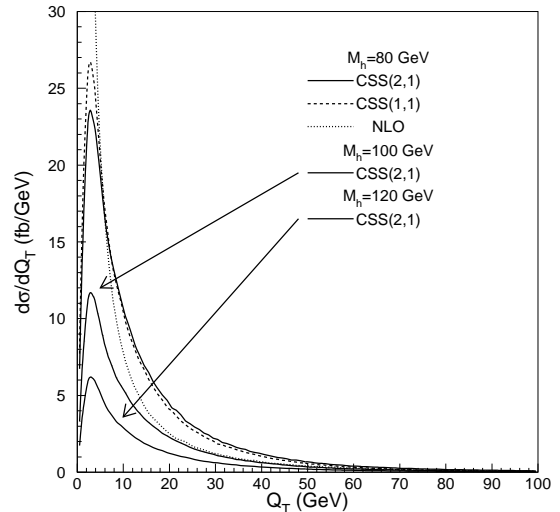


FIG. 1. The Q_T spectrum for W^+h Events

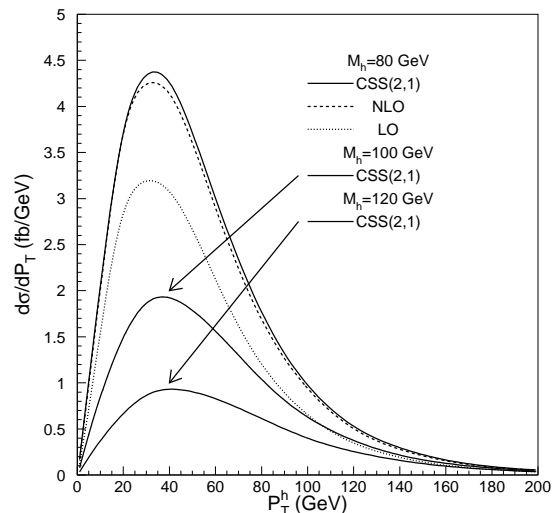


FIG. 2. The P_T^h spectrum for W^+h Events

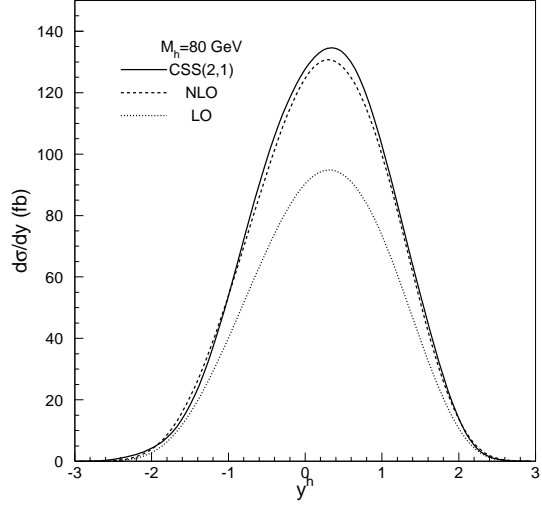


FIG. 3. The y^h spectrum for W^+h Events

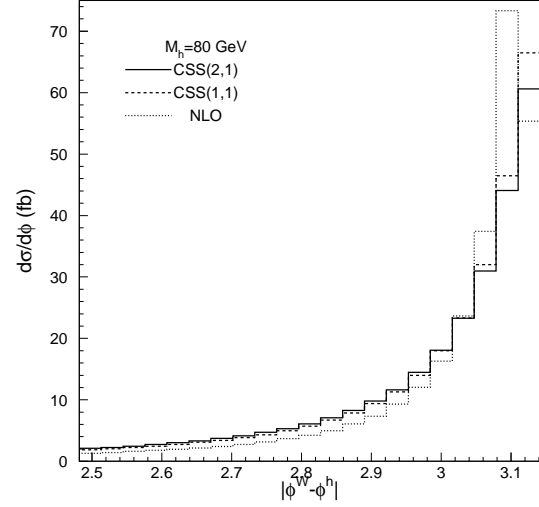


FIG. 5. The $\Delta\phi^{W^+h}$ spectrum for W^+h Events

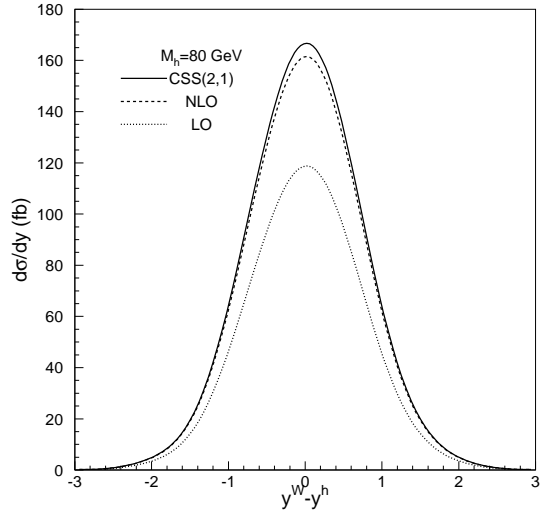


FIG. 4. The Δy^{W^+h} spectrum for W^+h Events

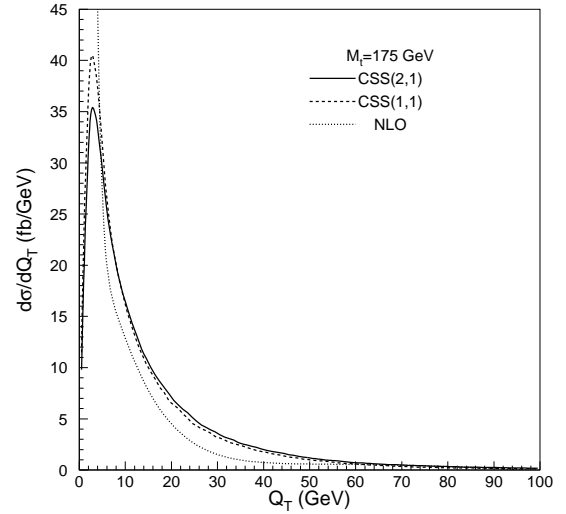


FIG. 6. The Q_T spectrum for $t\bar{b}(g)$ Events

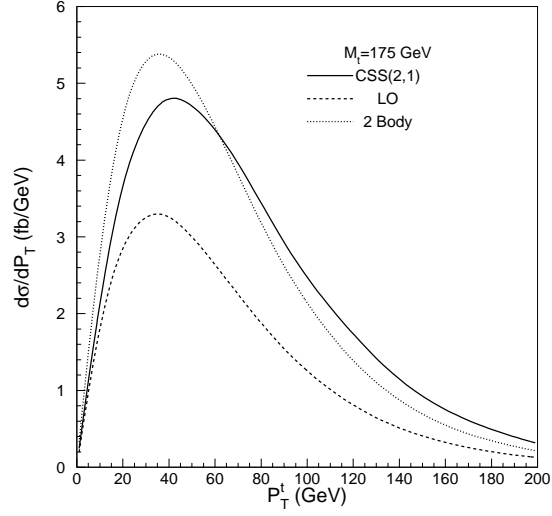


FIG. 7. The P_T^t spectra for $t\bar{b}(g)$ Events

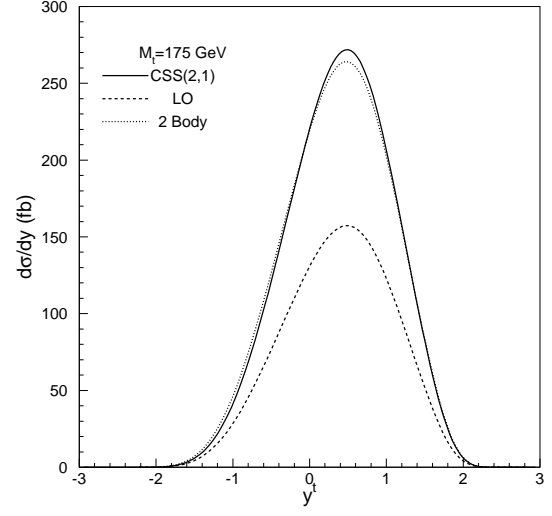


FIG. 9. The y^t spectrum for $t\bar{b}(g)$ Events

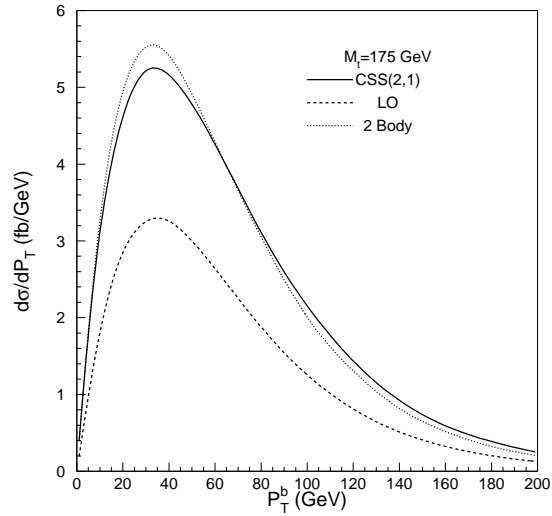


FIG. 8. The P_T^b spectra for $t\bar{b}(g)$ Events

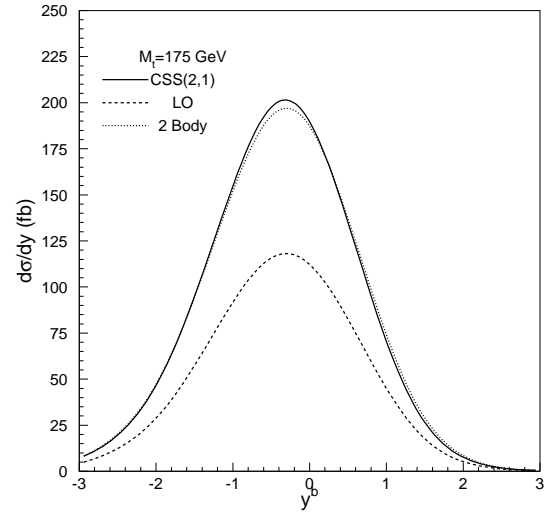


FIG. 10. The y^b spectrum for $t\bar{b}(g)$ Events

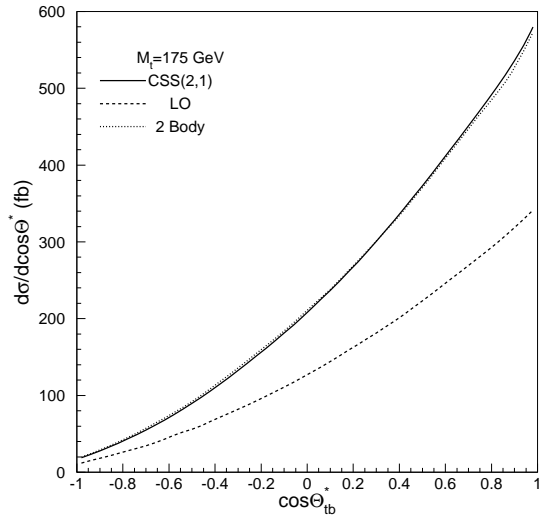


FIG. 11. The $\cos \theta_{t\bar{b}}^*$ spectrum for $t\bar{b}(g)$ Events

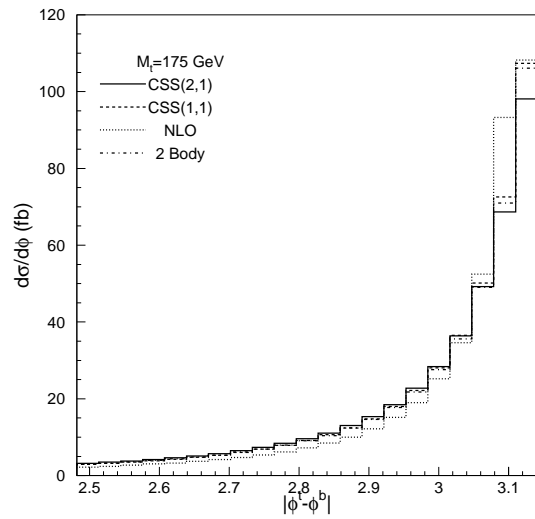


FIG. 12. The $\Delta \phi^{t\bar{b}}$ spectrum for $t\bar{b}(g)$ Events

